



An instrument to determine the magnetophoretic mobility of labeled, biological cells and paramagnetic particles

Jeffrey J. Chalmers^{a,*}, Yang Zhao^a, Masayuki Nakamura^a, Kristie Melnik^b,
Larry Lasky^b, Lee Moore^c, Maciej Zborowski^c

^a*Department of Chemical Engineering, The Ohio State University 140 W 19 Ave Columbus, OH 43210, USA*

^b*Department of Pathology, The Ohio State University 140 W 19 Ave Columbus, OH 43210, USA*

^c*Department of Biomedical Engineering, The Cleveland Clinic Foundation, 1900 Euclid Ave Cleveland, OH 44195, USA*

Abstract

An instrument is described and discussed which can determine the magnetophoretic mobility of immunomagnetically labeled cells and paramagnetic particles. Through the use of a well-characterized magnetic energy gradient and a computer algorithm, cell tracking velocimetry, it is possible to obtain the mean and distribution of the magnetophoretic mobility for samples with greater than 10^3 individuals. © 1999 Published by Elsevier Science B.V. All rights reserved.

Keywords: Magnetophoretic mobility; Immunomagnetic labeling; Cell tracking velocimetry

The ability to separate particles or biological cells that have paramagnetic characteristics has become a significant tool. Some of the earliest reports of the use of paramagnetism in separation are those of S.G. Frantz [1] from which two commercial devices for the separation of dry mineral particles were developed. More recently, the development of paramagnetic carriers, ranging from particles (micron size) to paramagnetic colloids (20–200 nm) (Miltenyi Biotec, Inc., Auburn, CA) linked to antibodies allows highly specific biological cell separations to be accomplished. In addition, a large number of other uses for these paramagnetic carriers exists, including: drug deliv-

ery, radionuclide therapy, contrast agents in MR imaging, and the separation of organelles, mRNA, genomic DNA, and proteins [2].

One can identify three primary factors which determine magnetic force acting on a magnetic carrier: the intensity of the magnetic energy gradient, the volume of the magnetic carrier, and the magnetic susceptibility of the magnetic carrier relative to the suspending medium. Mathematically, the magnetic force acting on a magnetic carrier is given by

$$F_b = \frac{1}{2\mu_0} \Delta\chi V_b \nabla B^2, \quad (1)$$

where F_b is the magnetic force acting on a single magnetic carrier, ∇B^2 is the magnetic energy gradient, V_b is the volume of the magnetic carrier, and

* Corresponding author. Tel.: +1 614-292-2727; Fax: +1 614-292-3769; e-mail: chalmers.1@osu.edu.

$\Delta\chi$ is the difference in magnetic susceptibility between the carrier and the suspending medium.

For a magnetic carrier moving in a liquid medium, this magnetic force is opposed by a hydrodynamic drag force. If the magnetic carrier moves sufficiently slow such that $Re < 1$, then one can assume that Stokes' Law applies and the drag resistance is represented by

$$F_d = 3\pi v_m D_m \eta, \quad (2)$$

where v_m is the velocity of the magnetic carrier, D_m is the diameter of the carrier, and η is the viscosity of the fluid.

If one makes the further assumption that forces due to gravity and buoyancy are negligible, conducting a force balance on the magnetic carrier, assuming a perfect sphere for the magnetic carrier, and setting the inertial term (mass times acceleration) equal to zero, one can obtain the following relationship for the velocity of a magnetic carrier in a magnetic energy gradient:

$$v_m = \frac{|\nabla B^2|}{2\mu_0} \frac{\Delta\chi D_m^2}{18\eta}. \quad (3)$$

In terms of separation technology, a 'normalized' parameter can be used which is analogous to electrophoretic mobility. This parameter, magnetophoretic mobility, μ_m , is the magnetically induced velocity divided by the magnetic energy gradient. Mathematically, it is represented by

$$\mu_m = \frac{v_m}{|\nabla B^2|/2\mu_0} = \frac{\Delta\chi D_m^2}{18\eta}. \quad (4)$$

As discussed in the assumptions used to obtain Eq. (4), it was assumed that the paramagnetic carrier was on the order of a micron in diameter. However, numerous examples of colloidal, submicron paramagnetic carriers which can range from 20 to several hundred nanometers exist. For example, with respect to cell separation, several commercial, paramagnetic carriers are available, such as those marketed by Miltenyi Biotec GmbH (Bergisch-Gladbach, Germany). These 20–150 nm colloidal carriers are conjugated to antibodies that either directly or indirectly bind to specific cell surface markers. In the case of cluster of differentiation, (CD), markers on human lymphocytes, 10^4 – 10^5 of

these cell surface markers exist per cell. If one assumes a saturation of the antigen binding sites and a minimum of one bead per antigen then at least 10^4 – 10^5 , [3] 20–150 nm paramagnetic carriers are bound per cell. The use of these colloidal carriers leads to a different mathematical analysis than that performed above when micron size carriers are used. Specifically, the magnetic force operating on a labeled cell, F_c , can be represented by

$$F_c = A_c \alpha \beta F_b, \quad (5)$$

where A_c is the surface area of a sphere the diameter of the cell, α is the number of cell surface markers per unit surface area to which the antibody–magnetic carrier conjugate can bind, β is the number of antibody magnetic carrier conjugates binding per cell surface marker, and F_b is, as before, the force acting on a single magnetic carrier. As above, this magnetic force acting on the labeled cell is opposed by a drag force given by Eq. (2) with the diameter of the magnetic carrier, D_m , replaced with the diameter of the labeled cell, D_c . Again, if the forces of gravity and buoyancy are ignored, combining Eqs. (5) and (2), and substituting for the surface area of a sphere, one obtains for the velocity of a cell, v_c , labeled with antibody–magnetic carrier complexes:

$$v_c = \frac{D_c \alpha \beta F_b}{3\eta}. \quad (6)$$

Substituting Eq. (1) into Eq. (6) for the magnetic force acting on a single magnetic carrier, one obtains:

$$v_c = \left[\frac{D_c \alpha \beta}{3\eta} \frac{|\nabla B^2|}{2\mu_0} \right] \Delta\chi V_b, \quad (7)$$

Finally, in terms of magnetophoretic mobility, one can obtain

$$\mu_m = \frac{v_c}{|\nabla B^2|/2\mu_0} = \frac{D_c \alpha \beta}{3\eta} \Delta\chi V_b. \quad (8)$$

A fundamental assumption in the equations defining the magnetophoretic mobility of magnetic carriers (Eq. (4)) and labeled cells (Eq. (8)) is that the magnetic energy gradient, $|\nabla B^2|/2\mu_0$ term is a known function of the position at which the velocity is determined (constant in the simplest case). Unfortunately, practically speaking, the creation of a

constant, or even a well characterized $\nabla B^2/2\mu_0$ environment in which to preform experiments and/or separations is a complex task. This complexity is demonstrated by the lack of any known analytical devices, except for that which will be presented below, and only one separation design, the Frantz Isodynamic separator, in which the $\nabla B^2/2\mu_0$ is well characterized.

To determine the magnetophoretic mobility of a magnetic carrier, or a cell labeled with magnetic carriers, Eq. (4) or Eq. (8) indicate that either the velocity of a particle or cell in a well defined magnetic energy gradient is needed or fundamental parameters associated with the particle or cell are needed. Conversely, knowing the magnetophoretic mobility of a particle or cell, one can study these fundamental parameters which govern the magnetophoretic mobility. For example, with respect to the labeling of cells with antibody–paramagnetic colloids, one can study the number of cell surface markers on a cell by studying cell motion in the magnetic energy gradient.

Over the years, several different techniques have been used to approximate the magnetophoretic mobility of paramagnetic cells/particles. These techniques include the use of visual microscopic observations of the movement of cells and a stop watch [4]; Magneto-Cytometry [5,6] which determines the fraction of a population which is labeled; a ferrograph which indirectly measures the magnetophoretic mobility of immunomagnetically labeled cells [7]; and cell tracking velocimetry (CTV) in a well-defined magnetic energy gradient [8].

In the remainder of this paper, improvements in the last technique listed above, CTV, will be presented as well as results obtained with two cell systems.

Fig. 1 is a flow chart presenting the procedure by which magnetophoretic mobilities are determined. Fig. 2 is a diagram of the magnet flow channel arrangement. Fig. 2a and Fig. 2b are end and side views, respectively, showing the location of the poles pieces, magnets, and column (1 mm \times 1 mm ID) through which cells flow. Of particular note is the region where the magnetic force is predicted to be nearly constant in the y -direction and zero in the x -direction.

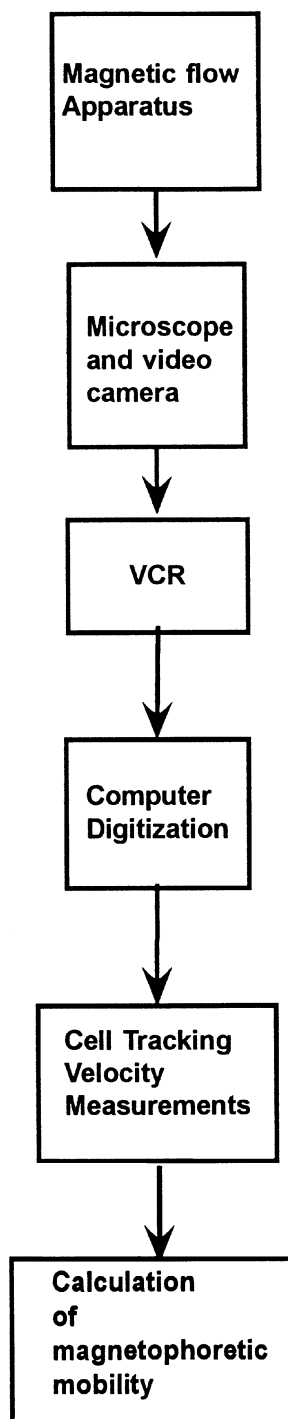


Fig. 1. Flow chart of the procedure used to obtain histograms of the magnetophoretic mobility of immunomagnetically labeled cells.

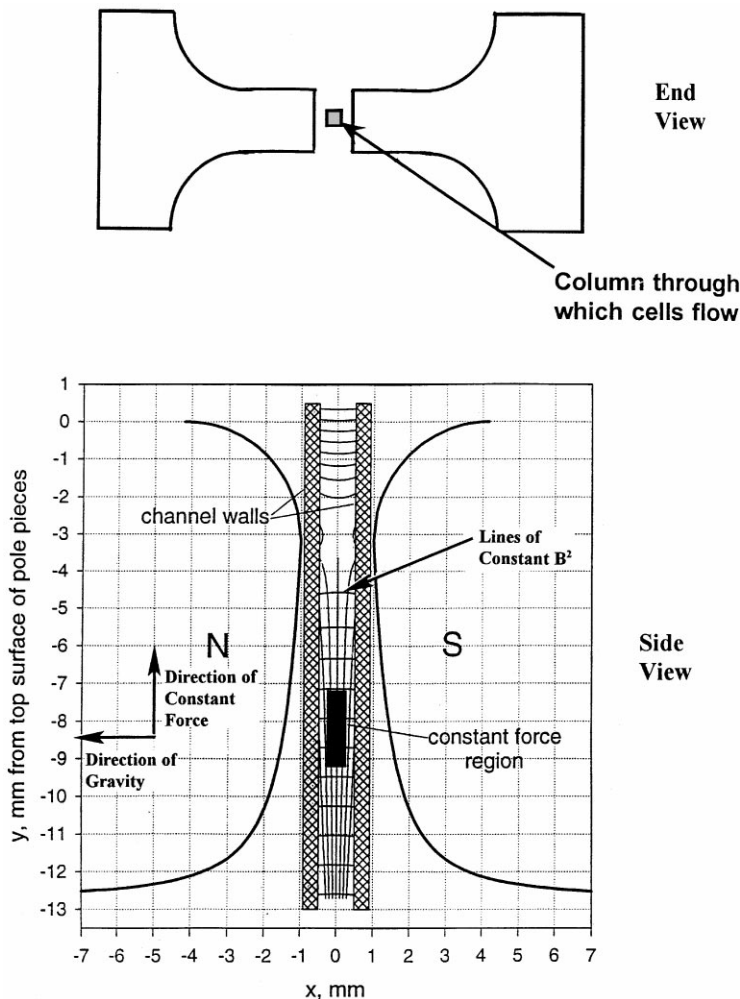


Fig. 2. Diagram of the magnetic flow channel system. (a) and (b) are end and enlarged side views. Horizontal, curved lines between the channel walls correspond to contours of B^2 while vertical lines correspond to lines of ∇B^2 .

The magnetic field is generated by two pairs of $2'' \times 2'' \times 1/2''$ of Ne-Fe-B magnets of maximum energy product of 2.23×10^5 T A/m. The pole pieces, which convey the flux through the air gap, are specially shaped in the x - y plane (see Fig. 2b) so that a constant energy gradient is achieved in a specific volume inside the flow channel. Magnetic field modeling software, Magneto (Integrated Engineering Software, Winnipeg, Manitoba) was used in the design of the magnetic assembly. The assembled magnetic system was evaluated by field measurements with a Gauss meter and Hall-effect probe

(F.W. Bell, Orlando, FL). The field measurements were then used to calibrate the software so that predicted and measured field strengths coincided.

Each of the remaining steps in the flow chart presented in Fig. 1 have been reported in previous publications [8,9]. Summarizing, this procedure uses microscopic video images to determine the velocity and position of each moving particle or cell. More recent modifications involve the use of more intense, and better positioned lighting which allowed the removal of some of the image processing steps after the video image is digitized by the

computer. This modification greatly simplifies the process and allows much more accurate data on both the location and velocity of the tracked cells or particles.

Two types of cells were used in the studies presented in this report: a genetically engineered strain of *Saccharomyces cerevisiae*, and human lymphocytes. The strain of *S. cerevisiae* was kindly provided by Professor Dane Wittrup of the University of Illinois. These cells have been engineered to express on the cell surface a fusion containing a scFv sequence and an epitope tag (c-myc) [10]. The procurement and preparation of human lymphocytes have been discussed previously [11].

A two-step labeling protocol was used and has been previously reported [11]. Briefly, it consists of the use of a primary antibody for the cell surface marker of interest and a secondary antibody directed for the primary antibody. Conjugated to the secondary antibody is a paramagnetic colloid. In

many cases a FITC molecule was conjugated to the primary antibody which facilitated fluorescence activated cell scanning (FACS) analysis. In the case of *S. cerevisiae*, the primary antibody used was an anti-myc mouse Mab (Berkeley Antibody Co., Richmond, CA).

Fig. 3 is a three-dimensional projection of the magnetic energy gradient in the y -direction. The figure was prepared by inputting Magneto-generated field data into Maple V software (Waterloo, Ontario). The Maple software then performed a five-point interpolation of the energy density, B^2 , obtaining $\partial B^2/\partial y$ (proportional to the y -direction magnetic force) at grid nodes over the specified x - y domain. As can be observed, the surface is nearly flat indicating that the magnetic force in the y -direction is predicted to be nearly constant in the observation area.

Fig. 4a presents predicted trajectory plots for immunomagnetically labeled cells within the region

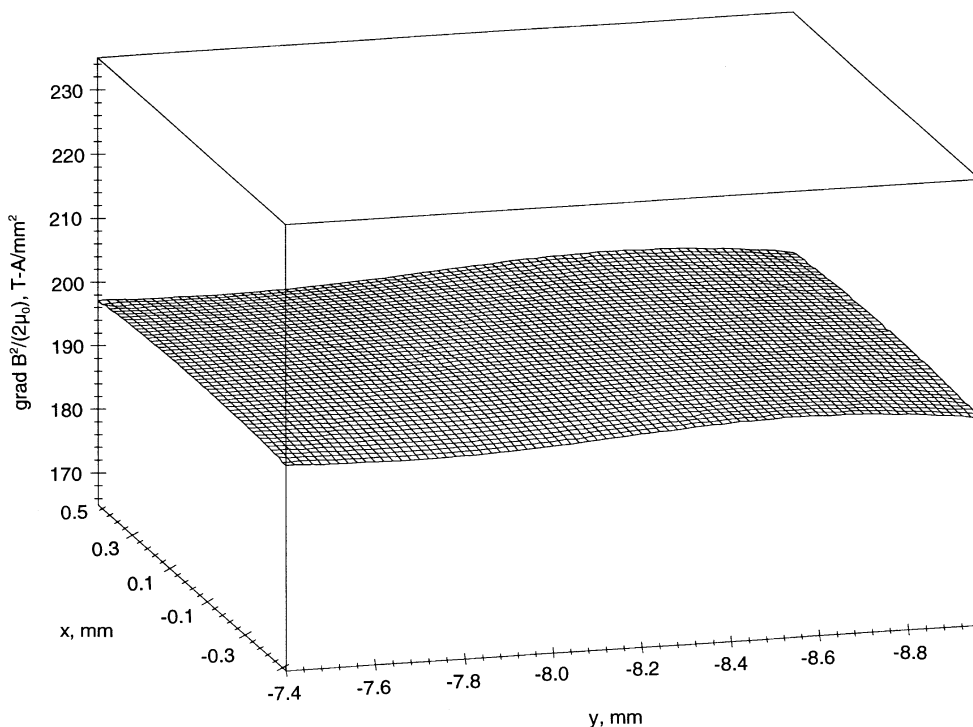


Fig. 3. A three-dimensional projection of the predicted magnetic energy gradient in the y -direction. The x and y coordinates refer to the region of predicted, nearly constant magnetic energy gradient (see Fig. 2b) and the z -axis is the magnitude of the predicted magnetic energy gradient in the y -direction.

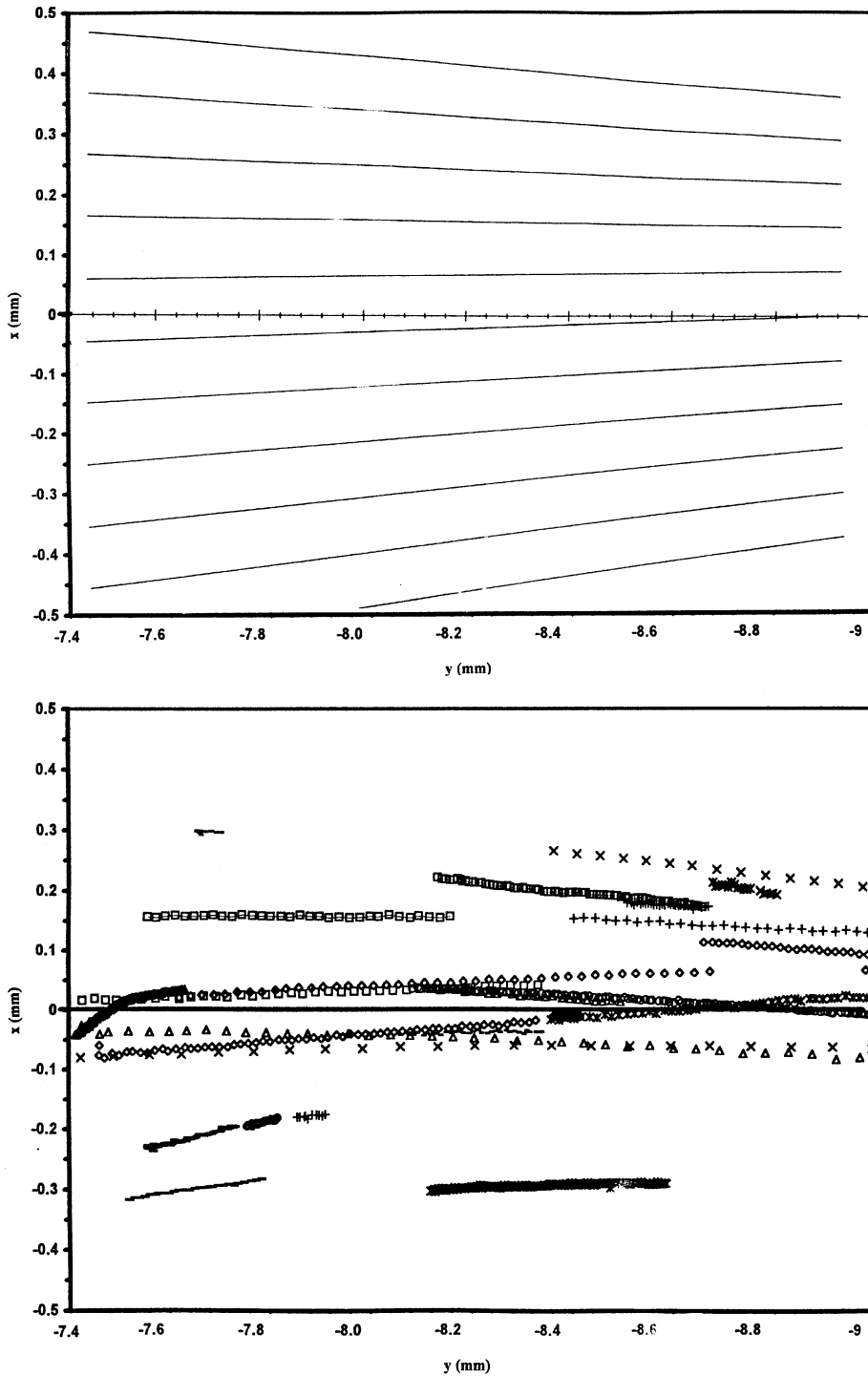


Fig. 4. Predicted, (a) and actual, (b), trajectory plots of immunomagnetically labeled cells in the region of predicted, constant magnetic energy gradient. The direction of motion is from right to left. The predicted trajectories were made using an average cell diameter of $7.3 \mu\text{m}$, a density difference between the cell and fluid of 1.05, and a magnetophoretic mobility of $2.96 \times 10^{-4} \text{ mm}^3/\text{T A s}$.

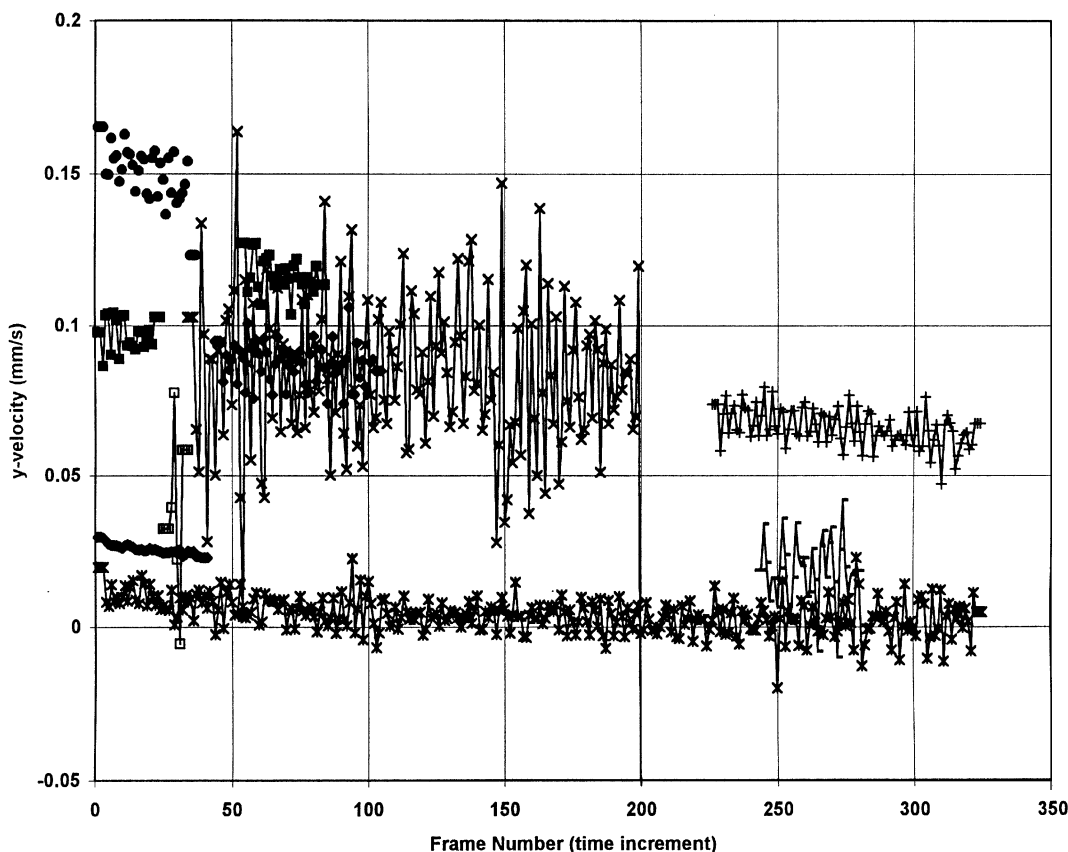


Fig. 5. Velocities of 10 immunomagnetically labeled lymphocytes randomly distributed in the region of predicted constant energy gradient. The y -axis is the y -component of the cell velocity and x -axis is the frame number.

shown in Fig. 3. The direction of motion is from right to left. These trajectory calculations were made for $7.3 \mu\text{m}$ cells, with a specific density of 1.05 and a magnetophoretic mobility of $2.96 \times 10^{-4} \text{ mm}^3/\text{T A s}$. As can be observed from these lines of trajectory (deflection off a straight line), the x component of the magnetic force slowly increases with the absolute value of the distance from the line of symmetry ($x = 0$). Fig. 4b is a plot of measured trajectories (using the CTV algorithm) of 25 randomly distributed immunomagnetically labeled human lymphocytes in the same region as shown in Fig. 4a. Tracks with symbols close together indicate slow movement while symbols more widely separated indicated a higher cell velocity. In addition, in a couple of cases, the tracks rapidly drop (move in negative x -direction). It is hypothesized that these

tracks are the result of clumps of cells which have been visually observed to drop more rapidly than single cells. However, further work is needed to investigate this observation.

Fig. 5 is a plot of the y -component of the velocity as a function of frame number for 10 (from a set of 50), randomly selected, immunomagnetically labeled lymphocytes. This y -component of the velocity is in the direction of predicted, constant magnetic energy gradient. As can be observed, the number of frames that a cell is tracked varies, depending on location and other factors. Also, in some cases significant fluctuations in the velocity is observed from frame to frame. These fluctuations are most likely the result of errors associated with the computer algorithm locating the center of the cell in each frame. Changes in the contrast between

the cell and the background can result in slight, but significant, changes in the calculated cell size, and corresponding cell center, which is used to calculate velocities. Consequently, in all cases an average of cell velocity was used.

Since a fundamental assumption in this work is that the magnetic energy gradient is constant in the y -direction (See Fig. 2), a verification of this assumption would be to determine if the velocity of a tracked cell is constant in the y -direction. A linear regression was performed on each of the 50 tracked cells described in the previous paragraph. From these linear regressions, predictions were made regarding the change in velocity from beginning to end of the track. Averaging these 50 predictions, it was determined that the final velocity of each track was 90% of the velocity at the beginning of the track. The source and true significance of this change has not been determined yet.

Fig. 6a is a histogram ($n = 1163$) of the magnetophoretic mobility for CD45 labeled human lymphocytes. The magnetophoretic mobility was obtained by dividing the CTV determined y -component of the cell velocity (mm/s) by the magnitude of the magnetic energy gradient, $|\nabla B^2|/(2\mu_0)$, 198 T A/mm^2 . Two significant questions can be raised with respect to this histogram: (1) what are the contributions to this histogram of background movement of the cells due to being pumped into the region of observation, and (2) what are the contributions to this histogram of any non-specific binding of the secondary antibody to the cells? Fig. 6b is a histogram ($n = 333$) of the residual cell velocity, in terms of magnetophoretic mobility, of unlabeled human lymphocytes after being pumped into the system. Fig. 6c is a histogram ($n = 491$) of the residual velocity of human lymphocytes with only the secondary antibody incubation (negative control of the primary antibody specificity). Fig. 7 is a histogram ($n = 1394$) of human lymphocytes labeled with a mouse anti-CD8 antibody and the same anti-mouse secondary antibody magnetic colloid conjugate.

In addition to the lymphocyte studies, experiments were conducted using the yeast expression system discussed previously. In these experiments, as opposed to the human lymphocyte studies, the cells were pumped into the system in the opposite

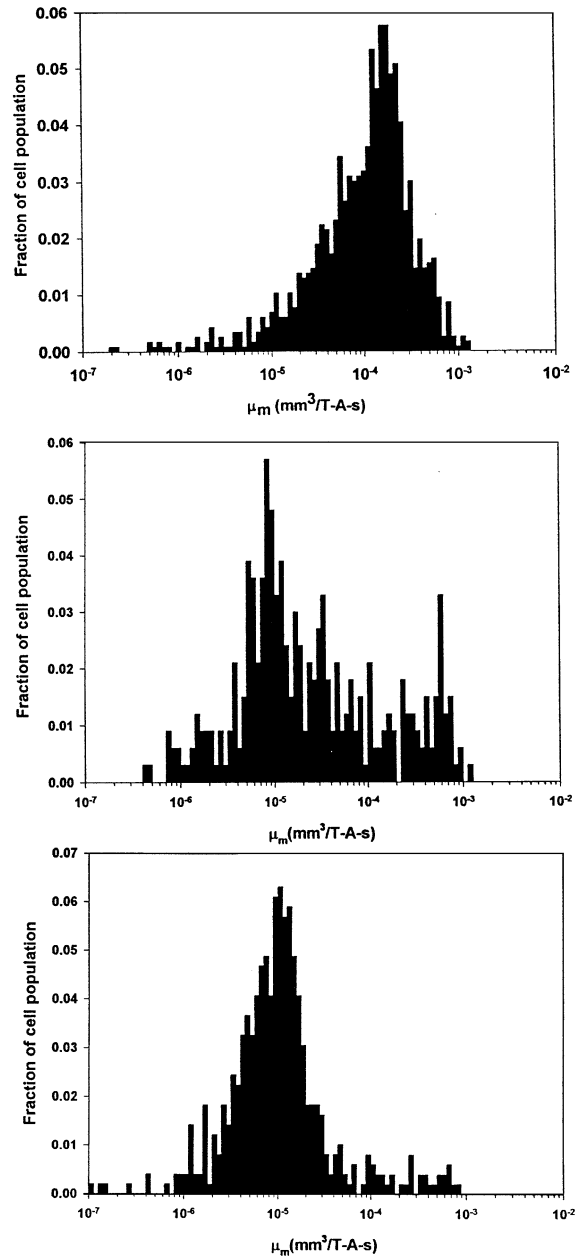


Fig. 6. (a) is a histogram of magnetophoretic mobility of immunomagnetically labeled, CD45 human lymphocytes. (b) is a histogram on the magnetophoretic mobility of unlabeled lymphocytes and (c) is a histogram of the results of an experiment in which the primary antibody was omitted.

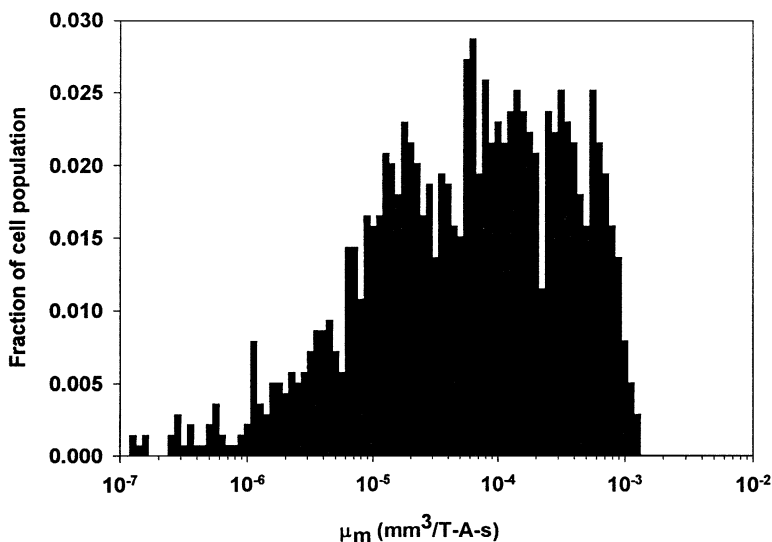


Fig. 7. A histogram of the magnetophoretic mobility of immunomagnetically labeled CD8 human lymphocytes.

direction relative to the magnetic force. In this mode of operation, any residual velocity in the cells would act opposite to the magnetic force and appear distinct from the magnetically induced velocity. Fig. 8a is a histogram ($n = 1160$) of immunomagnetically labeled *S. cerevisiae*. As indicated, approximately 70% of the cell population had a magnetophoretic mobility less than 10^{-8} mm³/T A s. Since a logarithmic histogram does not allow negative values to be presented, the lowest value 'bin' includes cells which would have a 'negative velocity' presumably remaining from the bulk flow into the channel. Fig. 8b is a histogram with only values of magnetophoretic mobility greater than 10^{-8} mm³/T A s.

A significant contribution of this work, relative to previous work, is the use of a magnetic system in which the region in which visual observations of the movement of immunomagnetically labeled cells are made has a nearly constant magnetic energy gradient. This greatly simplifies the determination of the magnetophoretic mobility of a labeled cell or particle.

As indicated by Eq. (7), any increase or decrease in the magnetic energy gradient, $\nabla B^2/2\mu_0$, would result in a change in the velocity of an immunomag-

netically labeled cells. As reported in the results section, an average decrease of 10% was observed in the velocity of a tracked cell from the first to last frame. This decrease is most probably due to a slight decrease in the magnetic energy gradient in the region of observation. It should be noted that the tracked cells were randomly distributed in the region of interest. The fluctuations in the velocity from frame to frame which can be observed in Fig. 5 are most probably the result of errors in the CTV software locating the center of a cell from frame to frame. Changes in contrast between the cell and background, or the movement of the cell out of the field of focus of the objective make the cell appear larger or smaller when the video image is digitized by the computer. This change in size, and subsequent change in the location in the center of the cell (which is used to calculate the velocity) can result in significant changes in velocity from frame to frame.

Fig. 6 indicates that significant differences in magnetophoretic mobility can be detected between immunomagnetically labeled cells and control samples. As a point of reference, in the system reported in this paper, values of μ_m of 10^{-5} , 10^{-4} , and 10^{-3} (mm³/T A s) correspond to velocities of $1.98 \times$

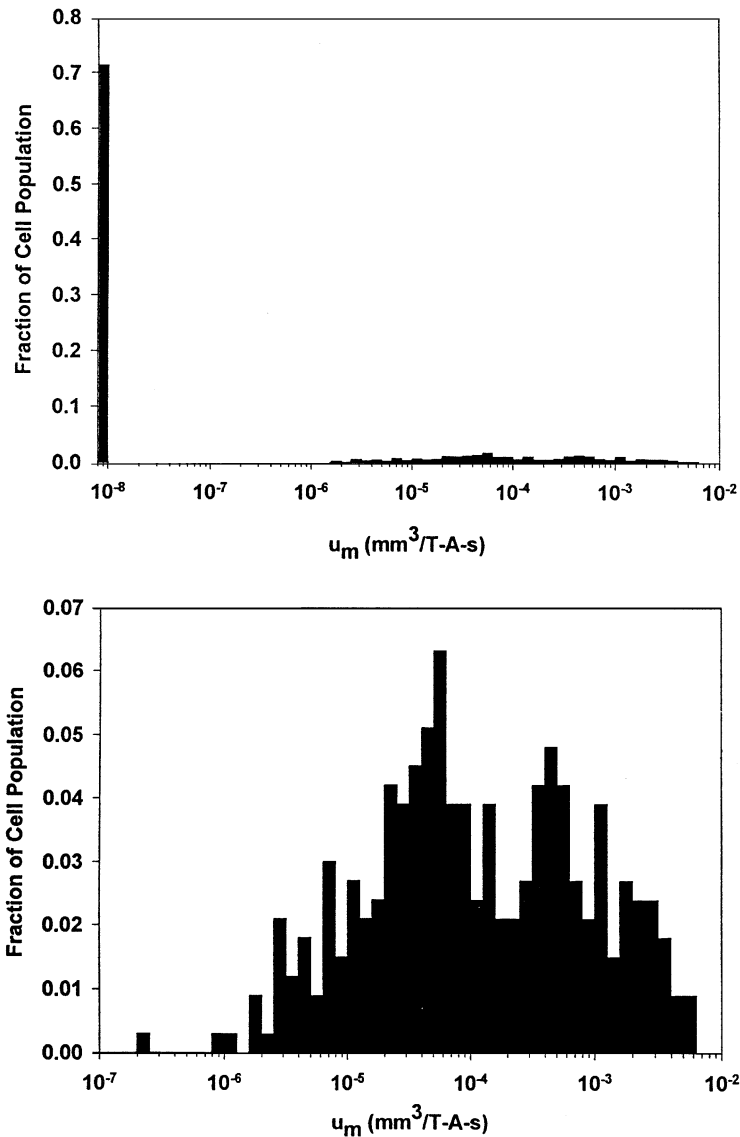


Fig. 8. (a) is a histogram of the magnetophoretic mobility of immunomagnetically labeled *S. cerevisiae* cells and (b) is a histogram of the data in with a magnetophoretic mobility greater than 10^{-8} $\text{mm}^3/\text{T A s}$.

10^{-3} , 1.98×10^{-2} , and 1.98×10^{-1} mm/s . As can be observed, Fig. 6c has less noise than Fig. 6b. While the data in Fig. 6c and Fig. 6a were generated at the same time, the data in Fig. 6b were generated previously and the operator's technique has significantly increased with respect to how cells are injected into the viewing region. This is an active

area of development in our lab and we are continuing to improve this technique.

As indicated by the *S. cerevisiae* data in Fig. 8, significantly greater differences between the background mobility and the labeled cell mobility can be obtained if the cells are pumped into the system in a direction opposite the direction that the

magnetic energy gradient operates on the cells. This observation indicates the importance of further improvements of the introduction of cells into the viewing region.

The purpose of this paper was to present an improved version of our system to quantify the magnetophoretic mobility of immunomagnetically labeled cells. Future improvements will involve the creation of a 'real time' system in which images of the moving cells are processed immediately by the computer. This will allow more studies to be conducted including a large number of binding studies to optimize the immunomagnetic labeling of cells. Other improvements will involve the better definition of background magnetophoretic mobility so that quantitative statements can be made with respect to any non-specific binding of immunomagnetic labels to cells.

This work was supported by the NIH (R01 CA62349), the Whitaker Foundation, and the National Science Foundation (BCS9258004).

References

- [1] S.G. Frantz 1936. US Patent 2,056,426.
- [2] M. Bosnes, A. Deggerdal, A. Rian, L. Korsnes, F. Larsen, in: U. Hafeli, W. Schutt, J. Teller, M. Zborowski (Eds.), *Scientific and Clinical Applications of Magnetic Carriers*, Plenum Press, New York, 1997.
- [3] A.N. Barclay, M.L. Brown, A.D. Beyers, S.J. Davis, C. Somoza, A.F. Williams, *The leukocytes antigen facts book*, Academic Press, San Diego, CA, 1993.
- [4] S.J. Gill, C.P. Malone, M. Downing, *Rev. Sci. Instr.* 31 (1960) 1299.
- [5] S. Winoto-Morbach, V. Tchikov, W. Muller-Ruchholtz, *J. Clin. Lab. Anal.* 8 (1994) 400.
- [6] S. Winoto-Morbach, V. Tchikov, W. Muller-Ruchholtz, *J. Clin. Lab. Anal.* 9 (1995) 42.
- [7] M. Zborowski, C.B. Fuh, R. Green, L. Sun, J.J. Chalmers, *Anal. Chem.* 67 (1995) 3702.
- [8] J.J. Chalmers, S. Haam, Y. Zhao, K. McCloskey, L. Moore, M. Zborowski, *Biotechnol. Bioeng.* in press.
- [9] S. Reddy, L.R. Moore, L. Sun, M. Zborowski, J.J. Chalmers, *Chem. Eng. Sci.* 51 (1996) 947.
- [10] E.T. Boder, K.D. Wittrup, *Nature Biotechnol.* 15 (1997) 553.
- [11] J. Chalmers, M. Zborowski, L. Sun, L. Moore, *Biotechnol. Prog.* 14 (1998) 141.